Journal of Power Sources xxx (2016) 1–11

Contents lists available at ScienceDirect

Journal of Power Sources

journal homepage: www.elsevier.com/locate/jpowsour

An ether-functionalised cyclic sulfonium based ionic liquid as an electrolyte for electrochemical double layer capacitors

Alex R. Neale [a], Sinead Murphy [a], Peter Goodrich [a], Christoph Schütter [b], Christopher Hardacre [a], Stefano Passerini [b], Andrea Balducci [b], Johan Jacquemin [a, *]

[a] School of Chemistry and Chemical Engineering, David Keir Building, Queen's University Belfast, Belfast, Northern Ireland BT9 5AG, United Kingdom
[b] Helmholtz Institute Ulm, Karlsruhe Institute of Technology, Helmholtzstraße 11, 89081 Ulm, Germany

HIGHLIGHTS

- A novel ether-functionalised cyclic sulfonium IL, [THT_{G1}][TFSI], was synthesised.
- Transport properties promoted by ether moiety relative to an alkyl-based analogue.
- Electrochemical/thermal stability [THT_{G1}][TFSI] not inhibited by ether moiety.
- [THT_{G1}][TFSI] used as solvent-free electrolyte in EDLC at 2.6 V.

ARTICLE INFO

Article history:
Received 29 January 2016
Received in revised form
12 May 2016
Accepted 17 June 2016
Available online xxx

Keywords:
Electrolyte
Ionic liquid
Sulfonium
Supercapacitor

ABSTRACT

A novel cyclic sulfonium cation-based ionic liquid (IL) with an ether-group appendage and the bis{(trifluoromethyl)sulfonyl}imide anion was synthesised and developed for electrochemical double layer capacitor (EDLC) testing. The synthesis and chemical-physical characterisation of the ether-group containing IL is reported in parallel with a similarly sized alkyl-functionalised sulfonium IL. Results of the chemical-physical measurements demonstrate how important transport properties, *i.e.* viscosity and conductivity, can be promoted through the introduction of the ether-functionality without impeding thermal, chemical or electrochemical stability of the IL. Although the apparent transport properties are improved relative to the alkyl-functionalised analogue, the ether-functionalised sulfonium cation-based IL exhibits moderately high viscosity, and poorer conductivity, when compared to traditional EDLC electrolytes based on organic solvents (propylene carbonate and acetonitrile). Electrochemical testing of the ether-functionalised sulfonium IL was conducted using activated carbon composite electrodes to inspect the performance of the IL as a solvent-free electrolyte for EDLC application. Good cycling stability was achieved over the studied range and the performance was comparable to other solvent-free, IL-based EDLC systems. Nevertheless, limitations of the attainable performance are primarily the result of sluggish transport properties and a restricted operative voltage of the IL, thus highlighting key aspects of this field which require further attention.

1. Introduction

Electrochemical double layer capacitors (EDLCs), or supercapacitors, stand among the most promising energy storage technologies today [1]. EDLCs store energy by charge separation at the electrode/electrolyte interface rather than by reversible redox reactions as in metal ion batteries [2]. To date, the major challenge for EDLCs when compared to other energy devices is their limited energy density (<10 Wh kg^{-1}) [3], which currently is unable to meet the requirements of high energy density applications. To overcome this challenge, extensive work has been undertaken to increase the energy density of EDLCs which has been the subject of a number of recent reviews [3–7]. As the energy density is proportional to the capacitance and the square of the voltage, increasing the capacitance and/or the cell voltage is an effective way to increase the energy density. This can be achieved through the development of novel carbon materials for electrodes with high capacitance, such as templated carbide-derived carbons [8,9],

* Corresponding author.
E-mail address: johan.jacquemin@qub.ac.uk (J. Jacquemin).

http://dx.doi.org/10.1016/j.jpowsour.2016.06.085

carbon nanotube-based structures [10,11] and graphene-derived carbons [12]. Furthermore, alternative materials may be selected for the electrode structure to introduce pseudocapacitive charging contributions. These materials may combine transition metal oxides with conductive polymer coatings, such as Co_3O_4 in polypyrrole [13] and $MnFe_2O_4$ in polyaniline [14], which, by incorporating redox active pseudocapacitive processes, may increase the total achievable capacitance. Alternatively, the development of novel electrolytes with increased operating potential windows is an important strategy for improving the energy storage capabilities of devices relying on purely capacitive charge storage. Currently, the majority of commercial EDLCs use organic electrolytes based on acetonitrile or propylene carbonate (with a tetraethylammonium tetrafluoroborate, $[Et_4N][BF_4]$, salt) with a cell operating voltage of 2.5–2.8 V [3,15]. While the utilisations of these electrolyte formulations have been studied in-depth and optimised for application in EDLCs, the ultimate performance may be hindered by the limited solubility of traditional salts in the solvents. A higher solubility salt can be used to form more concentrated electrolytes to promote better electrolyte conductivities and limit the possible electrolyte depletion at the interface [3]. Additionally, higher salt concentrations within the electrolyte can be utilised to reduce the potentially hazardous volatility and flammability of such solvents and, in turn, improve the safety of an operating EDLC [16].

In this regard, ionic liquids (ILs) are presently considered as attractive electrolyte materials for the development of safer EDLCs due to their intrinsic chemical-physical properties including their non-volatility and good (electro)chemical stability. Recent studies indicate that applying ILs as EDLC electrolytes, such as 1-ethyl-3-methylimidazolium tetrafluoroborate, $[EMIm][BF_4]$, and 1-butyl-1-methylpyrrolidinium bis{(trifluoromethyl)sulfonyl}imide, $[Pyrr_{14}][TFSI]$, operative voltages of up to 3.7 V can be achieved [17–19]. However, as ILs exhibit higher viscosities and lower conductivities than electrolytes based on organic solvents, IL-based EDLCs typically display lower power outputs than conventional EDLCs, especially under ambient operating conditions [20]. In recent years several strategies have been proposed to improve the power of IL-based EDLCs, focusing on the use of mixtures of ILs and organic solvents to be one of the most effective approaches. These mixtures have included conventional solvents, propylene carbonate and acetonitrile [19,21–23], and several reports of novel solvents including a variety of mononitriles [24], adiponitrile (an aliphatic dinitrile solvent) [25,26], gamma butyrolactone [27] and amides [28]. In general, the introduction of the solvent is used to promote the transport capabilities of the electrolyte relative to the neat IL while still maintaining high concentrations of the ionic species and, in turn, improve capacitance of the IL-based EDLCs at high currents under ambient conditions.

Other approaches towards the improvement of ILs as electrolytes for EDLCs and other electrochemical energy storage devices can involve judicious tailoring of the cation-anion functionality to manipulate the chemical-physical properties of the IL. For example, incorporation of ether appendages (*e.g.* substitution of a butyl side chain for a similarly sized 2-methoxyethyl group) can in some instances contribute to the decrease of viscosity and melting point without drastically impacting on the electrochemical and thermal stability [29–31]. Similarly, careful selection of the structure of the anionic component, for example bulky fluorine-based anions with highly delocalised electron distributions, may be utilised to tailor the chemical-physical properties of the resulting IL [29,31]. For example, in view of an IL consisting of a 1-butyl-1-methylpyrrolidinium cation with a $[TFSI]^-$ anion (bulky, high charge delocalisation, flexible), the melting point and viscosity (254 K and 76 mPa s at 298 K, respectively) is significantly lower than for the analogous IL with a symmetrical, non-flexible $[BF_4]^-$ anion where the negative charge is more localised and the melting point is 423 K [29]. Alternatively, the application of ILs based on the fluorine-free dicyanamide anions, $[N(CN)_2]^-$, in EDLCs has also recently been reported [32]. In combination with pyrrolidinium based cations, the $[N(CN)_2]^-$-based ILs were reported to exhibit lower viscosity and higher conductivity than the $[TFSI]^-$-based analogues and, in turn, displayed very good power capabilities, and good capacity retention over 25,000 cycles when used as solvent-free EDLC electrolytes. Nevertheless, the electrochemical stability, and the operative voltage, of the $[N(CN)_2]^-$-based ILs was reported as lower than the $[TFSI]^-$ analogues, potentially limiting the available energy density of EDLC based on such an IL electrolyte.

Cations suitable for the implementation of innovative ILs include those based on sulfur which typically display lower viscosities in comparison to their analogous ammonium counterparts [33,34]. For example, at 298 K the reported viscosity and conductivity of $[TFSI]^-$-based ILs with an *S*-butyl-*S*-dimethylsulfonium cation (39.0 mPa s and 10.0 mS cm^{-1} at 298 K, respectively) is significantly improved relative to *N*-butyl-*N*-triethylammonium $[TFSI]^-$ (104.1 mPa s and 6.9 mS cm^{-1}, respectively); an analogous tetraalkylammonium cation-based IL of approximately similar size [34]. However, despite having a lower viscosity, higher conductivity and lower melting points, ILs based on trialkylsulfonium cations have attracted limited attention compared to their ammonium analogues. Nevertheless, several groups have reported work emphasising the use of cyclic [35–38] and acyclic [39–41] sulfonium ionic liquids as electrolytes for energy devices. Research surrounding the influence of ether functionalisation of the cation on the properties of sulfonium-based ILs has only been studied by Han et al. [42] wherein ILs based on the bis(fluorosulfonyl)imide anion, $[FSI]^-$, and small acyclic sulfonium cations with and without ether functionality were reported to exhibit low viscosities (20–30 mPa s at 298 K), good conductivities (8.2–15.7 mS cm^{-1} at 298 K) and reasonable electrochemical stability windows (*ca.* 4.2–4.8 V). Recently, we also reported the use of acyclic aprotic sulfonium ILs as potential electrolytes for EDLC devices [27].

With the aim to further develop and understand the limits related to the use of sulfonium-based ILs in supercapacitors, we investigated the chemical-physical properties of the alkyl and ether functionalised cyclic sulfonium ILs, *S*-butyltetrahydrothiophenium bis{(trifluoromethyl)sulfonyl}imide, $[THT_4][TFSI]$, and *S*-(2-methoxyethyl)tetrahydrothiophenium bis{(trifluoromethyl)sulfonyl}imide, $[THT_{G1}][TFSI]$. The electrochemical performance of EDLCs containing the novel ether-functionalised IL, $[THT_{G1}][TFSI]$, as a neat electrolyte was also investigated as a proof of concept.

2. Experimental

2.1. Synthesis

2.1.1. General synthesis of S-butyltetrahydrothiophenium bis{(trifluoromethyl)sulfonyl}imide, $[THT_4][TFSI]$, and S-(2-methoxyethyl)tetrahydrothiophenium bis{(trifluoromethyl)sulfonyl}imide, $[THT_{G1}][TFSI]$

The alkylating agent, 1-iodobutane (Sigma-Aldrich, 99%, 190.46 g, 1.035 mol, 1.0 eq.) or 2-bromoethyl methyl ether (Fluorochem, 95%, 143.86 g, 1.035 mol, 1.0 eq.), was added to a flask of tetrahydrothiophene (Sigma-Aldrich, 99%, 91.28 g, 1.035 mol, 1.0 eq.) with a small amount of acetone (Sigma-Aldrich, 99.8%). The reaction mixture was stirred vigorously, covered in aluminium foil and left to react for 72 h at 333 K to give the corresponding halide salts as a white solid. After filtration of the solid, each of the intermediate salts were analysed by ^1H NMR. These sulfonium halide salts were then mixed and stirred with a solution of lithium bis{(trifluoromethyl)sulfonyl}imide (3 M, battery grade) (205.84 g,

0.717 mol, 1.1 eq.) and (233.69 g, 0.814 mol, 1.1 eq.) for the iodide and bromide salts, respectively in 150 cm^3 of ultrapure water for 15 h at room temperature to facilitate the metathesis exchange reaction of halide ions with $[TFSI]^-$ ions. Thereafter, dichloromethane (Sigma-Aldrich, 99.5%) was added to dissolve the ionic liquid and the two phases separated. The viscous organic phase containing the IL, $[THT_4][TFSI]$ or $[THT_{G1}][TFSI]$, was then washed several times with 50 cm^3 fractions of ultrapure water to remove residual lithium halide salts. The dichloromethane was removed under reduced pressure on a rotary evaporator. A general reaction schematic is shown in Figure S1 in the Supporting Information. Prior to all further measurements, the ILs were dried under high vacuum (10^{-3} mbar) at elevated temperature (343 K) with stirring for several days. The ILs were subsequently stored in an Ar-filled glove box (<3 ppm H_2O) to limit water contamination by the ambient atmosphere. ^1H and ^{13}C NMR spectra were recorded at 293.15 K on a Bruker Avance DPX spectrometer at 300 MHz and 75 MHz, respectively, see Figures S2-S5 in Supporting Information. Lithium content was determined by inductively coupled plasma optical emission spectroscopy (ICP-OES) on an Agilent 5100 ICP-OES and, along with Microanalysis, were performed by Analytical Services at Queen's University Belfast.

2.1.2. S-butyltetrahydrothiophenium iodide, $[THT_4]I$

(Yield 63%, 177.47 g, 0.652 mol) ^1H NMR (300 MHz, $CDCl_3$) δ 4.10–3.83 (m, 2H), 3.82–3.45 (m, 4H), 2.54 (t, $J = 9.2$ Hz, 4H), 1.96–1.75 (m, 2H), 1.58 (dq, $J = 14.5$, 7.2 Hz, 2H), 1.00 (t, $J = 7.3$ Hz, 3H).

2.1.3. S-(2-methoxyethyl)tetrahydrothiophenium bromide, $[THT_{G1}]Br$

(Yield 71.5%, 167.87 g, 0.739 mol) ^1H NMR (300 MHz, $CDCl_3$) δ 3.72 (t, $J = 5.9$ Hz, 2H), 3.48 (t, $J = 6.0$ Hz, 2H), 3.41 (s, 3H), 2.83 (dd, $J = 8.4$, 4.4 Hz, 4H), 1.98–1.89 (m, 4H).

2.1.4. S-butyltetrahydrothiophenium bis{(trifluoromethyl)sulfonyl}imide, $[THT_4][TFSI]$

(Yield 95%, 263.50 g) ^1H NMR (300 MHz, DMSO) δ 3.50 (dt, $J = 12.6$, 6.3 Hz, 2H), 3.45–3.28 (m, 2H), 3.32 (s, 3H), 3.27–3.09 (t, $J = 9.0$ Hz 2H), 2.35–2.04 (m, 4H), 1.80–1.56 (dt, $J = 15.1$, 7.5 Hz, 2H), 1.43 (dq, $J = 14.3$, 7.3 Hz, 2H), 0.94 (t, $J = 7.3$ Hz, 3H). ^{13}C NMR (75 MHz, DMSO) δ 126.26 (s), 122.00 (s), 117.66 (s), 113.43 (s), 43.08 (s), 41.55(s), 28.34 (s), 26.78 (s), 21.30 (s), 13.48 (s). CHNS Theo%.: C, 28.23; H; 4.00, N, 3.29; S, 22.61; Exp%.: C, 28.30; H; 4.37, N, 3.49; S, 22.61. Li content <1 ppm.

2.1.5. S-(2-methoxyethyl)tetrahydrothiophenium bis{(trifluoromethyl)sulfonyl}imide, $[THT_{G1}][TFSI]$

(Yield 98% 303.25 g) ^1H NMR (300 MHz, DMSO) δ 3.83–3.72 (m, 2H), 3.62–3.40 (m, 6H), 3.35 (s, 3H), 2.36–2.08 (m, 4H).· ^{13}C NMR (75 MHz, DMSO) δ 126.26 (s), 121.87 (d, $J = 18.1$ Hz), 117.73 (s), 113.38 (d, $J = 12.3$ Hz), 66.78 (s), 58.60 (s), 28.32 (s). CHNS Theo%.: C, 25.29; H, 3.54; N, 3.28; S, 22.51; Exp%: C, 24.94; H, 3.22; N, 3.12; S, 22.19. Li content 10 ppm.

2.2. Physical measurements

Water content of the dried ILs was analysed by Karl Fischer Coulometric titration using an 899 Coulometer (Metrohm). The resolution of the water content measurements was 0.001 wt/wt % (or 10 ppm) and measurements were completed in duplicate. All ILs displayed water contents lower than 50 ppm H_2O after vacuum drying. Thermal gravimetric analysis (TGA) of the ILs was undertaken using a Q5000 TGA instrument (TA Instruments). The sample size was 5–10 μg for each IL. Heating was conducted from room temperature to 873 K (±1 K) applying a temperature gradient of 5 K min^{-1} using nitrogen as purge gas (10 cm^3 min^{-1}). Differential scanning calorimetry (DSC) analysis of the ILs was completed using a DSC Q2000 (TA Instruments) using a heating gradient of 5 K min^{-1} between lower and upper temperature limits of 183.15 K and 323.15 K (±0.1 K), respectively. IL samples for DSC were prepared in hermetically sealed Al pans inside an Ar-filled glove box.

Density measurements were completed at atmospheric pressure using a DM40 (Mettler Toledo, ± 1 × 10^{-4} g cm^{-3}) oscillating tube density meter in the range of 293.15–363.15 K (±0.1 K). The DM40 instrument was cleaned using acetone and dried using dehumidified air prior to any measurements. The viscosity of the ILs was measured using a Bohlin Gemini Rotonetic Drive 2 cone and plate rheometer (±1%) from *ca.* 293.15–363.15 K (±0.01 K) at atmospheric pressure. Density and viscosity measurements were completed under atmospheric conditions and, therefore, samples were sealed in glass vials inside the Ar-filled glove box and only exposed to the ambient atmosphere immediately before completion of the respective measurement to limit water contamination. Conductivity measurements were completed using a sensION + EC71 benchtop meter with a 3-pole platinum sensION+ 5070 conductivity probe (<0.5% of range) with an in-built Pt1000 temperature probe (Hach Lange). The conductivity probe was calibrated using aqueous KCl standard conductivity solutions (147 μS cm^{-1}, 1413 μS cm^{-1}, and 12.88 mS cm^{-1} at 298.15 K). The sample was prepared inside an Ar-filled glove box by immersion of the probe into the liquid sample in a glass sample tube and sealing using an O-ring seal and parafilm. The conductivity of the IL was then measured as a function of the temperature within the range of 293.15–363.15 K (±0.2 K). The temperature of the sample was controlled using a small oil bath and the temperature and conductivity of the sample was recorded when the observed values were stable for *ca.* 30 s.

2.3. Electrochemical measurements

2.3.1. Electrochemical window at glassy carbon electrodes

Measurements of the electrochemical stability windows by cyclic voltammetry were performed using a VMP multichannel potentiostatic-galvanostatic workstation (BioLogic Science Instruments). Measurements were conducted inside the dry atmosphere of the Ar-filled glovebox using a three-electrode configuration in a three-necked glass cell. The working electrode was a glassy-carbon macro-disk (ALS Co., Ltd., 3 mm diameter). Prior to all experiments, the glassy carbon working electrode was polished using alumina slurries of decreasing grain size (1.0 μm, 0.3 μm, and 0.05 μm) in distilled water. The electrode was then sonicated in distilled water for 2–3 min then dried at *ca.* 353 K in an oven. The counter electrode was platinum-coiled wire heat-sealed in a glass capillary. The Ag[OTf]/Ag reference electrode consisted of the silver wire immersed in a 0.01 mol dm^{-3} solution of silver triflate (Ag[OTf]) in 1-butyl-1-methylpyrrolidinium bis{(trifluoromethyl)sulfonyl}imide, $[Pyrr_{14}][TFSI]$, separated from the bulk solution by a glass-frit tip. The Ag[OTf]/Ag electrode potential was referenced *vs.* an internal ferrocene (Sigma-Aldrich, 98%) couple. The determination of the ferrocene redox couple was completed by cyclic voltammetry after adding a small quantity of ferrocene to the IL after measurement of the electrochemical window.

2.3.2. EDLC measurements

In order to assess the usability of $[THT_{G1}][TFSI]$ in EDLC application, the IL was tested with carbon based composite electrodes. For this procedure, electrodes were prepared following the procedure reported in Ref. [43] using activated carbon, AC, as the active

material. The final ratio between active material (DLC Super 30, Norit), conductive agent (SuperC65, Imerys) and binder (CMC, Walocel CRT 2000 PPA 12, Dow Wolff Cellulosics) was 90:5:5. The electrode thickness was equal to 80 μm and the electrode diameter was 12 mm. The mass loading of the active material of the electrodes was, on average, 3.9 mg cm^{-2}. Free standing electrodes with mass loadings over 30 mg cm^{-2} were prepared using a different binder (polytetrafluoroethylene, PTFE, Sigma Aldrich) with a final composition of 85:10:5 (activated carbon, carbon black, PTFE). The aqueous PTFE dispersion, the activated carbon and the carbon black were dispersed in an excess amount of ethanol and stirred at elevated temperatures until the slurry became a highly viscous, dough-like mass. This mass was put onto a glass plate and rolled out several times before punching out disks with a diameter of 12 mm (area: 1.13 cm^2). The obtained electrodes were pre-dried in an oven (ED 115, Binder) set to 353 K, before drying them for 24 h under vacuum at 453 K, in order to remove any residual water.

Electrochemical tests were performed using a VMP multichannel potentiostatic-galvanostatic workstation (Biologic Science Instruments) connected to climatic chambers set to 293 K (KBF 115, Binder). The electrochemical investigations were carried out using Swagelok®-type cells, which were assembled in an Ar-filled glove box with water and oxygen contents below 1 ppm.

The maximum operative voltage of the electrolyte was determined in a three-electrode cell setup. An AC composite electrode was used as working electrode and a heavy and free standing AC electrode was used as counter electrode. As a reference electrode, an Ag quasi-reference electrode was employed. A Whatman GF/D glass microfiber filter disk (675 μm thickness and 13 mm diameter), soaked with 150 μL of electrolyte, was used as separator. The measurements were performed by cyclic voltammetry (CV), scanning the cell potential with a scan rate of 5 mV s^{-1}. Starting from a potential of 0.8 V/−0.8 V *vs*. Ag, the maximum potential was increased/decreased stepwise by 0.1 V until the efficiency of the CVs dropped below 99%.

In order to evaluate the performance of EDLCs with a [THT_{G1}][TFSI] electrolyte, CV and galvanostatic charge-discharge cycling experiments were carried out in a 2-electrode configuration using 100 μL of electrolyte and two AC composite electrodes. An asymmetric configuration with different electrode masses based on Equation (1) was used for this test using values of specific capacitance (C), carbon loading (m) and voltage excursion (ΔV) obtained by the 3-electrode configuration [44].

$$C^+ \cdot m^+ \cdot \Delta V^+ = C^- \cdot m^- \cdot \Delta V^- \quad (1)$$

Cyclic voltammetry was carried out using scan rates ranging from 5 mV s^{-1} to 200 mV s^{-1}. The reported values for specific capacitance correspond to the value achieved at the half of the maximum voltage and were normalised using the mass of the active material of both electrodes. Galvanostatic charge-discharge cycling was carried out using current densities ranging from 0.5 A g^{-1} to 5 A g^{-1}. The values of capacitance of the total active material (C), equivalent series resistance (ESR), Coulombic efficiency (η_{eff}), average energy (E) and average power (P) have been calculated using the formulas indicated in Refs. [43,45].

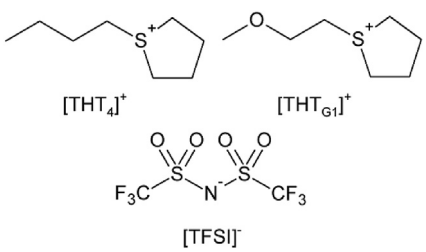

Fig. 1. Chemical structure of the *S*-butyltetrahydrothiophenium, $[THT_4]^+$, and *S*-(2-methoxyethyl)tetrahydrothiophenium, $[THT_{G1}]^+$ cations and the bis{(trifluoromethyl) sulfonyl}imide, $[TFSI]^-$, anion.

3. Results and discussion

The tetrahydrothiophenium bis{(trifluoromethyl)sulfonyl}imide based ILs were synthesised *via* alkylation of tetrahydrothiophene in moderate yield followed by subsequent metathesis of the resultant halide salts with Li[TFSI] in a dichloromethane/aqueous mixture. The ILs were purified by multiple washings with water to remove the halide and lithium residues followed by extensive drying under high vacuum. The chemical structures of the synthesised ILs, and their respective abbreviations, used in this work are shown in Fig. 1. A physical chemical characterisation of the two ILs was completed and the results are briefly summarised at 298.15 K in Table 1. Electrochemical characterisation and application of the ether functionalised IL in an EDLC in described in the latter stages of this work.

3.1. Physical characterisation

3.1.1. Thermal properties

Differential scanning calorimetry (DSC) and thermogravimetric analysis (TGA) of the ILs were used to study thermal phase transitions and thermal stability, respectively. As described in the experimental section, the DSC traces were completed within a range of 183.15 K and 323.15 K at a rate 5 K min^{-1}. Both ILs exhibited no distinct features associated with freezing or melting within this range at this heating rate. Accurate determination of the liquid range may require further experiments in which a slower heating rate and wider temperature range is utilised. In the low temperature region, both ILs showed evidence of a glass transition during the heating scan in the form of small broad peaks. The temperature at the mid-point of these peaks is used to define the glass transition temperature, T_g, for these ILs; *ca* 191 K for $[THT_4]$[TFSI] and 187 K for [THT_{G1}][TFSI]. The low temperature region of the DSC traces is shown in Figure S6 in the Supporting Information. The data presented in the traces show that these peaks appear very close to the switching temperature (183.15 K), particularly for the [THT_{G1}][TFSI] IL. This factor may limit the accuracy of determination of this peak position, especially since T_g peaks are broad. Nevertheless, the relative comparison of the ILs shows that the introduction of ether functionality depresses the T_g. This observation is possibly attributed to higher rotational freedom and flexibility of the ether group

Table 1
Thermal and physicochemical properties of $[THT_4]$[TFSI] and [THT_{G1}][TFSI] at 298.15 K.

Ionic liquid	M_w/g mol^{-1}	T_g/K	T_d/K	H_2O/ppm	V_m/cm^3 mol^{-1}	ρ/g cm^{-3}	η/mPa s	σ/mS cm^{-1}	Λ/S cm^2 mol^{-1}
$[THT_4]$[TFSI]	425.43	191	523	<50	292.23	1.4558	85.37	2.49	0.73
[THT_{G1}][TFSI]	427.41	187	554	<30	280.95	1.5231	70.38	3.01	0.85

M_w is the IL molecular weight, T_g and T_d are the glass transition temperature and thermal decomposition temperature, respectively, ρ is the density, η is the viscosity, σ is the conductivity, Λ is the molar conductivity and V_m is the molar volume.

Please cite this article in press as: A.R. Neale, et al., Journal of Power Sources (2016), http://dx.doi.org/10.1016/j.jpowsour.2016.06.085

and, for example, has been reported for $[TFSI]^-$-based ILs with *N*-butyl-*N*,*N*-diethyl-*N*-methylammonium (T_g = 180 K) and *N*,*N*-diethyl-*N*-(2-methoxyethyl)-*N*-methylammonium (T_g = 178 K) [31].

For the TGA experiments, the temperature is increased at a rate of 10 K min^{-1} giving dynamic information about the sample mass change in response to high temperatures. Results of the TGA analysis are shown in Figure S7 in the Supporting Information. For this analysis, the decomposition temperature (T_d) is the temperature at which a 5% loss in the sample weight is recorded. The measured T_d for the alkyl and ether-functionalised ILs is 523 K and 554 K, respectively. The recorded value for $[THT_4][TFSI]$ is slightly lower than has been reported previously for the thermal decomposition of a series of alkyl functionalised tetrahydrothiophenium $[TFSI]^-$ based ILs (which ranged from 545 to 550 K) [37]. This may be the result of several contributing factors; different pan materials, trace level impurities (including water) for example. Nevertheless, these results importantly show that the substitution of the ethereal oxygen into the functional group, does not negatively affect the relative thermal stability of the IL and it is, therefore, sufficiently thermally stable for practical electrochemical energy storage devices.

In addition, the combination of DSC and TGA measurements facilitates the approximation of the lower and upper temperature limits of the liquid ranges of the ILs. For the $[THT_4][TFSI]$ and $[THT_{G1}][TFSI]$ ILs, respectively, this range is estimated from the observed T_g at 191 K and 187 K to the observed T_d at 523 K and 554 K. These upper limits are considerably larger than is observed for conventional solvents, acetonitrile and propylene carbonate, for which significant electrolyte loss observed *via* evaporation even at temperatures well below 400 K [46,47]. However, the upper limits of the liquid range of the sulfonium-based ILs reported in this work are slightly lower compared to some commonly utilised ILs. For example, the decomposition temperature for $[Pyrr_{14}][TFSI]$ and [EMIm][TFSI] has been reported as greater than 673 K (400 °C) [48,49]. Conversely, the lower limits of the liquid temperature range of the cyclic sulfonium ILs reported in this work are estimated to exceed commonly used pyrrolidinium and imidazolium-based ILs with the $[TFSI]^-$ anion. For example, $[Pyrr_{14}][TFSI]$ and [EMIm][TFSI] are reported to melt at 260 K [50] and 252 K [26], respectively, which are considerably higher than the glass transition temperatures observed for both the alkyl and ether functionalised thiophenium ILs reported here. While these observations were completed using dynamic techniques, the results suggest the possibility of the application of this class of tetrahydrothiophenium-based ILs as electrolytes in low-temperature EDLCs.

3.1.2. Density

The densities of the sulfonium-based ILs were measured as a function of the temperature within the range of 293.15–363.15 K. The temperature dependence on the measured density, ρ, and the molar volume, V_m, (calculated using the density and molar mass) for both ILs is presented in Fig. 2. As is expected for ILs, the density of both samples was found to decrease with a linear dependence with respect to increasing temperature. As such, the data is fitted using the linear fitting equation

$$\rho = A + BT \tag{2}$$

where T is the sample temperature and A and B are the coefficients of the linear fit. The fitting parameters used in the linear correlation are shown, with the numerical density data, in Table S1 in the Supporting Information. Additionally, a logical increase in the molar volume of both ILs is observed with increasing temperatures. The experimental density of the butyl functionalised IL, $[THT_4][TFSI]$, at 298 K (1.4558 g cm^{-3}) is in excellent agreement with previously reported values (1.46 g cm^{-3} and 1.456 g cm^{-3}) at the same temperature [36,37]. Substitution of the butyl chain with the similarly sized 2-methoxyethyl group creates an IL with similar molecular weight but leads to tighter packing and a more dense IL. This trend has been observed previously for alkyl/ether-functionalised imidazolium, ammonium and phosphonium-based ILs [29–31,51,52].

Furthermore, the isobaric coefficient of thermal expansion, α_p, of the sulfonium ILs was calculated using Equation (3).

$$\alpha_p = \frac{1}{V_m}\left(\frac{\partial V_m}{\partial T}\right)_p = -\frac{1}{\rho}\left(\frac{\partial \rho}{\partial T}\right)_p \tag{3}$$

For $[THT_4][TFSI]$ and $[THT_{G1}][TFSI]$, the α_p values obtained at 298 K were 6.59×10^{-4} K^{-1} and 6.64×10^{-4} K^{-1}, respectively. Since the observed temperature dependence of density and molar volume appears to be linear across the studied temperature range, minimal deviation in the calculated α_p values is found. These calculated values are in good accordance with α_p values previously

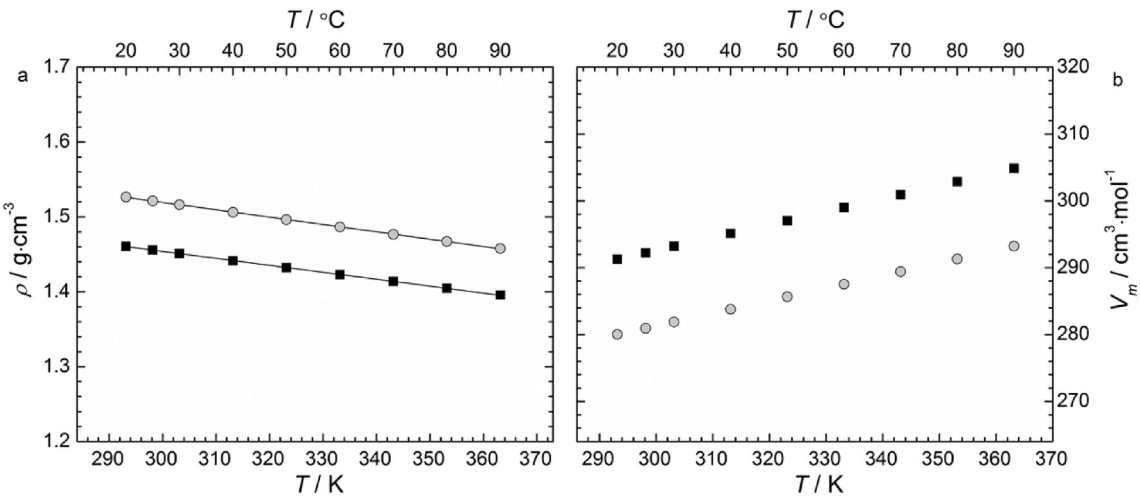

Fig. 2. Temperature dependence of the measured density (a) and molar volume (b) of the $[THT_4][TFSI]$ (■) and $[THT_{G1}][TFSI]$ (○). Solid lines represent the correlation of the density data using the linear fitting equation, $\rho = A + BT$.

reported for a series of $[TFSI]^-$-based ILs including [EMIm][TFSI] (6.50×10^{-4} K^{-1} at 293.15 K) and $[N_{4111}][TFSI]$ (6.34×10^{-4} K^{-1} at 293.15 K), where $[N_{4111}]^+$ is a *N*-butyl-*N*,*N*,*N*-trimethylammonium cation [53].

3.1.3. Viscosity and conductivity

The viscosity and conductivity of EDLC electrolytes is of particular importance for the high-power capabilities demanded by the application. Since viscosity is a property linked to the movement of the constituent molecules of the liquid, low viscosity electrolytes are required to enable good conductivity and rapid response of the ionic species to applied polarisation at the electrode interface. Both the viscosity and conductivity of an IL electrolyte contribute significantly to the maximum specific power, P ($W \cdot kg^{-1}$), of a given EDLC, as shown in Equation (4) [3]:

$$P = \frac{U_{max}^2}{4 \cdot ESR \cdot m} \tag{4}$$

where U_{max} is the maximum operative potential range in volts, m is the mass of the EDLC in kg and the *ESR* is the equivalent series resistance in ohms. The *ESR* is a summation of the different contributions to resistance of the EDLC, including electrode/electrolyte interfacial resistances and ionic resistance (reciprocal of the electrolyte ionic conductivity). Therefore, low viscosity and high ionic conductivity electrolytes are favoured for minimizing excessive contributions to the ESR. Since the operative potential range of ILs is characteristically high, it is the typically high viscosity and poor conductivity which may limit the application of pure IL electrolytes.

The viscosity and conductivity of the ILs was measured as a function of temperature within the range of 293.15–363.15 K. The temperature dependence of the viscosity and conductivity for the two tetrahydrothiophenium ILs is presented in Fig. 3. Both ILs exhibited a non-linear reduction in the measured viscosity with respect to an increase in the sample temperature. In accordance with the typical inverse proportionality observed between viscosity and conductivity, the measured conductivity of both ILs is found to increase with a non-linear dependence on the sample temperature. Correlation of the temperature dependence of the data was completed using the Vogel-Tamman-Fulcher, VTF, equations for viscosity, η (Equation (5)), and for conductivity, σ (Equation (6)):

$$\eta = \eta_o exp\left(\frac{B_\eta}{T - T_o^\eta}\right) \tag{5}$$

$$\sigma = \sigma_o exp\left(\frac{B_\sigma}{T - T_o^\sigma}\right) \tag{6}$$

where η_o, B_η, T_o^η and σ_o, B_σ, T_o^σ are fitting parameters for the viscosity and conductivity correlation, respectively, and T is the experimental temperature. The VTF equations are typically utilised for correlation of the temperature dependencies of conductivity and viscosity for glassy-forming liquids which do not obey Arrhenius-type dependence [54]. The correlation parameters, and the

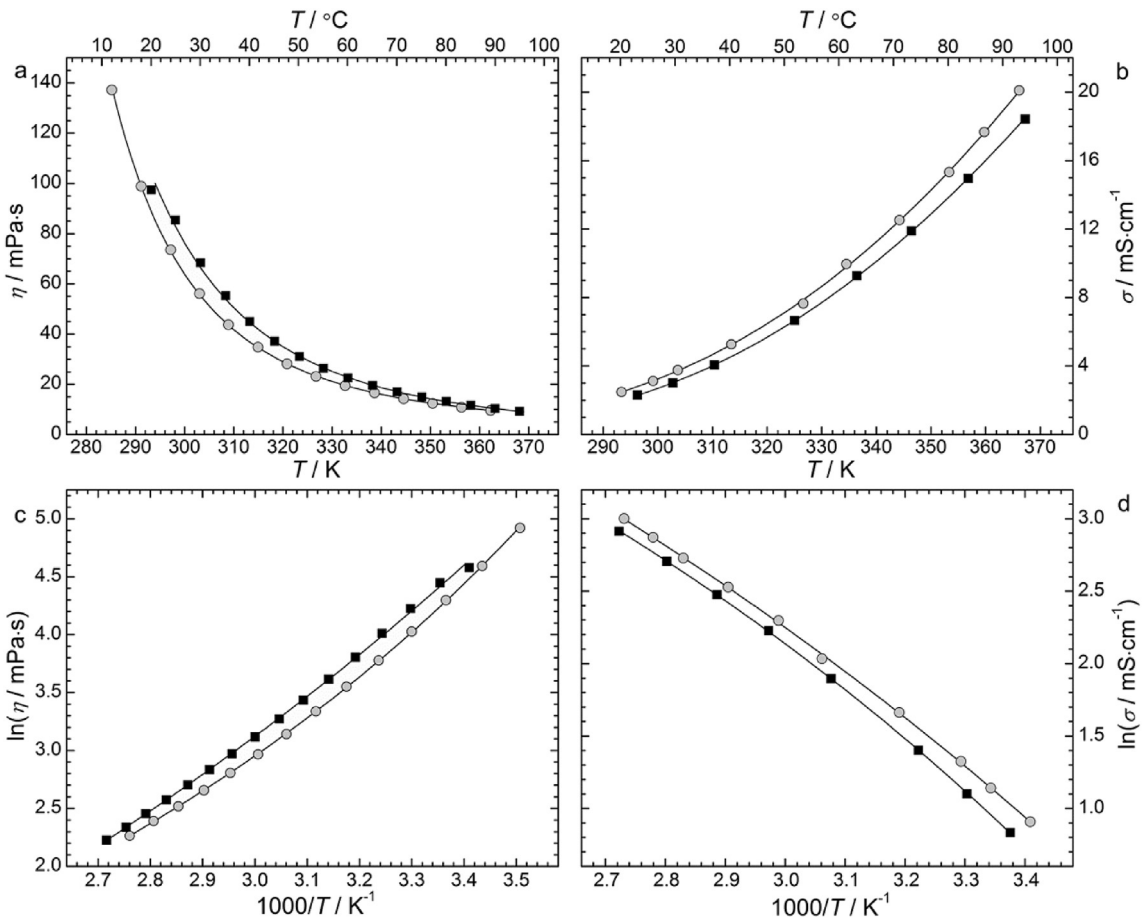

Fig. 3. Temperature dependence on the viscosity (a) and the conductivity (b), and the respective Arrhenius-type plots (c, d), of $[THT_4][TFSI]$ (■) and $[THT_{G1}][TFSI]$ (◎). Solid lines represent correlation of the data using the VTF fitting equations (Equations (5) and (6)).

numerical viscosity and conductivity data, are shown in Tables S2 and S3 in the Supporting Information. Across the full temperature range, the viscosity of the ether-functionalised IL, [THT_{G1}][TFSI], is found to be lower than for the butyl-functionalised analogue. As discussed previously, the substitution of a short alkyl substituent chain on an IL cation centre with a similarly sized ether group has been previously reported to result in a reduction of the IL viscosity [29–31,52,55]. In accordance with the reduction in the viscosity, the measured conductivity of the ether-functionalised IL is higher than for the alkyl-functionalised analogue. This observation is expected due to the similarities between the nature and the size of the IL structures. Nevertheless, under ambient conditions (298 K), both neat ILs exhibit higher viscosities ([THT_4][TFSI] = 85.37 mPa s, [THT_{G1}][TFSI] = 70.38 mPa s) and lower conductivities ([THT_4][TFSI] = 2.48 mS cm^{-1}, [THT_{G1}][TFSI] = 3.00 mS cm^{-1}) in comparison to a benchmark EDLC electrolyte, 1 mol dm^{-3} [Et_4N][BF_4] in propylene carbonate (2.6 mPa s and 13 mS cm^{-1}, respectively) [21].

For the butyl-functionalised IL, [THT_4][TFSI], the measured viscosity and conductivity shows a degree of variation with respect to previously reported values. Table 2 shows comparisons of the viscosity and conductivity values reported in this work with data available in the literature in the case of [THT_4][TFSI]. It is common for significant degrees of variation to occur between reported viscosity and conductivity values possibly owing to several factors including experimental technique and low-level impurities. One such impurity, which may significantly contribute to differing reports of ILs transport properties, is the water content (listed in Table 2 where available in the respective referenced articles). Higher water content in an IL may reduce the observed viscosity and, in turn, promote the conductivity of the solution. For the viscosity measurements reported in this work, and the comparative references, experimental measurements were conducted under ambient atmosphere without any moisture control. Therefore, the actual water content at the time of measurement would vary depending on the conditions of the atmosphere and the exposure time. As described in the experimental section, the IL samples were sealed in a glass vial with a septum inside an Ar-filled glove box and only exposed to atmosphere when added *via* a syringe and needle to the cone and plate rheometer. Taking this factor into consideration, the variation in the apparent viscosity measurements follows an approximate trend in-line with the IL water content. Conversely, no such trend may be inferred for the conductivity data and, in particular, the highest reported value of 3.2 mS cm^{-1} is in combination with the highest measured viscosity at the lowest recorded temperature which ultimately appears paradoxical. For the conductivity measurements reported in this work, the IL sample and probe were sealed inside a glass sample tube using an O-ring seal and parafilm while inside the Ar-filled glove box. This method has been tested previously using a range of different IL samples and no observable changes to the measured conductivity occurred over a period of 48 h.

3.1.4. Ionicity

To further probe the ionic behaviour and the inverse relationship between the exhibited viscosities and conductivities of the two tetrahydrothiophenium ILs, the ionicity of the ILs may be considered [57]. The degree of ionicity, or degree of (dis)association of the ionic species, is a description of the extent to which the ionic species within the IL behave as free and dissociated ions. A simple inspection of this feature is made using a Walden plot of $Log_{10}(\eta^{-1})$ *vs.* $Log_{10}(\Lambda)$, where the reciprocal viscosity (or fluidity), η^{-1}, is given in $Poise^{-1}$ and the molar conductivity, Λ (where $\Lambda = \sigma$ ($S \cdot cm^{-1}$)/*concentration* ($mol \cdot cm^{-3}$)), is given in $S \cdot cm^2 \cdot mol^{-1}$. The concentration was calculated using measured density and the molar mass of the IL. The Walden plot for the two tetrahydrothiophenium ILs in the temperature range of 293.15–363.15 K is shown in Fig. 4. Specific data points on the Walden plot are calculated using the correlation parameters of the density, viscosity and conductivity and the molecular weight of each IL. The solid line represents the ideal Walden behaviour of a 0.01 mol dm^{-3} KCl aqueous solution, a strong electrolyte solution in which the ionic species are known to be fully dissociated and equally mobile [58]. The magnitude and direction of deviation away from this ideal KCl line is said to describe the degree of ionicity of the studied materials. For example, an IL which lies well below the KCl line will exhibit a much lower-than-expected conductivity for the given viscosity according to the Walden rule. Where this deviation, ΔW (where ΔW represents the magnitude of the vertical displacement from the ideal KCl line) is greater than an order of magnitude lower than the ideal KCl line ($\Delta W > 1$), these ILs have been described as poorly ionic as a result of various interionic associations [57,59,60]. Conversely, ILs which lie close to the ideal KCl line, and ΔW is small,

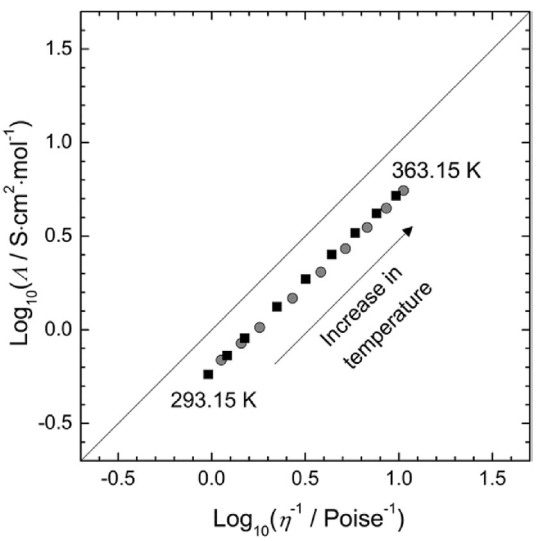

Fig. 4. Walden plot of the [THT_4][TFSI] (■) and [THT_{G1}][TFSI] (◎) ILs.

Table 2
Comparison of the viscosity and conductivity data of [THT_4][TFSI] reported in this work with previously reported literature data. Reported water content is also shown where available.

η/mPa s	σ/mS cm^{-1}	*Reported temperature*/K	*Reported water content*/ppm	Reference
85.37	2.48	298	<50	This work
104.8 (94.4)[a]	3.2	293	50.3	[36]
53.60	2.43	298	187	[37]
74	2.3	298	[b]	[56]

[a] Value in brackets corresponds to an estimation of the reported viscosity of the IL at 298 K based on the provided Arrhenius correlation ($\eta = A \cdot \exp(E_a/RT)$) parameters given in the respectively referenced article (E_a = 36.44 kJ mol^{-1} and $A = 3.9 \times 10^{-5}$ mS cm^{-1}).
[b] =Not reported. The number of significant figures provided for the literature values is exactly as provided by the authors of the respective articles.

show more dissociated ionic character in which the constituent ions are more independently mobile. Both the alkyl and ether-functionalised tetrahydrothiophenium based ILs reported in this work show small deviations away from the ideal line ($\Delta W > 0.3$) across the full temperature range representing '*good ionic liquids*' in which the ionic species are mostly dissociated and mostly move independently.

Nevertheless, both of the studied tetrahydrothiophenium-based ILs display a decrease in the calculated Walden-like product ($\Lambda{\cdot}\eta$) with increasing temperature ranging from *ca.* 60×10^{-7} S N·s·mol^{-1} at 293.15 K to 53×10^{-7} S N s mol^{-1} at 363.15 K for [THT_4][TFSI] and 60×10^{-7} S N s mol^{-1} to 52×10^{-7} S N s mol^{-1} for [THT_{G1}][TFSI] over the same range. The magnitude of these values is in good agreement with other previously reported [TFSI]$^-$-based ILs [61] including [$Pyrr_{14}$][TFSI] ($\Lambda{\cdot}\eta = 56$ S N s mol^{-1} at 298 K). This variation in calculated $\Lambda{\cdot}\eta$ is additionally in accordance with a slight increase in the observed ΔW over the same temperature range and demonstrates a lower gradient of both apparent linear dependencies relative to the ideal KCl line. While this variation is minimal over the studied temperature range, the observations imply that the conductivity of both ILs does not increase at the rate expected from the measured reduction in IL viscosity. Furthermore, the slight difference in the magnitude of ΔW for the two ILs may be discussed in terms of the different cation structures. Firstly, the only difference in IL structure is the substitution of the butyl group of the cation for the ether group which results in a slight increase in ΔW for the latter example. In comparison to the alkyl group, the ether moiety is more electron donating and, in turn, is more able to donate electron density towards the positively charged sulfur centre of the cation. As such, the charge distribution of the [THT_{G1}]$^+$ cation is expected to be more localised around the sulfur centre relative to the [THT_4]$^+$ cation. As an effect of this relatively small difference, a more localised positive charge would favour stabilisation through Coulombic interaction with the anionic species forming ion pairs and, in turn, reducing the apparent ionicity of the IL.

3.2. Electrochemical measurements

3.2.1. Electrochemical window at a glassy carbon electrode

One of the primary benefits of utilising ILs for electrochemical energy storage devices, in addition to the safety aspects related to non-volatility and non-flammability, is the typically wide electrochemical stability. Electrochemical stability of electrolytes is defined by the positive and negative potentials, in volts, at which the onset of oxidative or reductive decomposition reactions, respectively, occur at the electrode/electrolyte interface. In turn, the potential window defined by these upper and lower potential limits to give the electrochemical window of the electrolyte. The electrochemical window of the [THT_4][TFSI] and [THT_{G1}][TFSI] was measured by cyclic voltammetry at 2 mV s^{-1} at a glassy carbon working electrode and the resulting voltammograms are presented in Fig. 5. For the purpose of comparison of the specific potentials, the Ag[OTf]/Ag reference potential was normalised *vs.* the formal redox potential of an internal ferrocene couple (Fc^+/Fc). Additionally, low current boundaries of ±0.03 mA cm^{-2} to define the onset potential of electrolyte decomposition.

As seen in Fig. 5, both ILs exhibit one large negative current response at approximately −2.0 to −2.2 V *vs.* Fc^+/Fc associated with reductive decomposition of the ILs, most likely reduction of the cation species. In the anodic oxidative region, both ILs exhibit a significant oxidative current at approximately 2.25–2.35 V *vs.* Fc^+/Fc. In addition to this, a small positive current response is observed at *ca.* 1.8 V *vs.* Fc^+/Fc in the [THT_4][TFSI] IL, most likely associated with oxidation of trace level amounts of impurity. The numeric

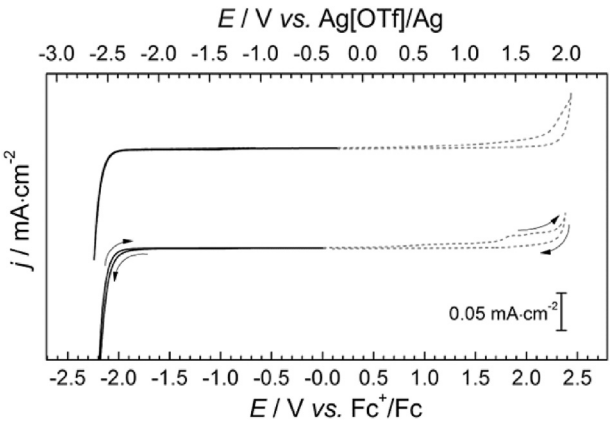

Fig. 5. Electrochemical windows of the [THT_4][TFSI] (bottom) and [THT_{G1}][TFSI] (top) ILs at a glassy carbon working electrode *vs.* a Ag[OTf]/Ag reference electrode (top X-axis) and normalised *vs.* an internal reference potential of the ferrocene redox couple (bottom X-axis). Scan rate was 2 mV s^{-1}.

anodic (E_a) and cathodic (E_c) potentials of oxidation and reductive decomposition, respectively, and the electrochemical window ($\Delta E = (E_a - E_c)$ V) are presented in Table 3. Additionally, in comparison with the previously reported electrochemical stability window of the [THT_4][TFSI] (3.4 V), our results implies a significantly wider operative voltage for this IL. In comparison with previously reported acyclic trialkylsulfonium [TFSI]$^-$ based ILs (*e.g.* $\Delta E = 3.7$ V for *S*-butyl-*S*,*S*-diethylsulfonium-[TFSI]) [62], the electrochemical windows of the cyclic analogues reported in this work show wider and cleaner electrochemical stability windows (where the term *cleaner* refers to the absence of significant current responses in addition to the two primary decomposition peaks). In comparison with other IL families commonly utilised for electrochemical applications, the reductive stability is approximately 1 V more positive than typically reported for quaternary ammonium [52,63–65] and phosphonium [65–68] based aprotic ILs (*e.g.* $\Delta E = 5.8$ V and *ca.* 6 V for [$Pyrr_{14}$][TFSI] [64] and *P*-pentyl-*P*,*P*,*P*-triethylphosphonium-[TFSI] [68], respectively). Conversely, the reported magnitude of ΔE for the tetrahydrothiophenium ILs is on a similar scale to that reported for imidazolium [TFSI]$^-$-based ILs [51,69]. Nevertheless, the results presented in Fig. 5 importantly show that the introduction of ether-functionality to the cyclic sulfonium cation does not negatively affect the electrochemical stability relative to the alkyl-functionalised analogue.

3.2.2. EDLC measurements

After identifying the electrochemical stability window, the operative voltage of the [THT_{G1}][TFSI] IL was determined *via* completion of CV measurements using a 3-electrode setup with high surface area, EDLC-type electrodes. The CV curves as well as the corresponding efficiencies are presented in Fig. 6. The positive and negative potential limits were defined by the highest and lowest potential limits, at which the efficiency of the charge-discharge remained higher than 99%. Within this threshold, the IL

Table 3
Cathodic reduction potential (E_c), anodic oxidation potential (E_a) and electrochemical windows (ΔE) of the alkyl and ether functionalised tetrahydrothiophenium bis{(trifluoromethyl)sulfonyl}imide ILs at a planar glassy carbon working electrode.

IL cation	E_c/V *vs.* Fc^+/Fc	E_a/V *vs.* Fc^+/Fc	ΔE/V
[THT_4]$^+$	−2.09	2.32	4.41
[THT_{G1}]$^+$	−2.15	2.27	4.42

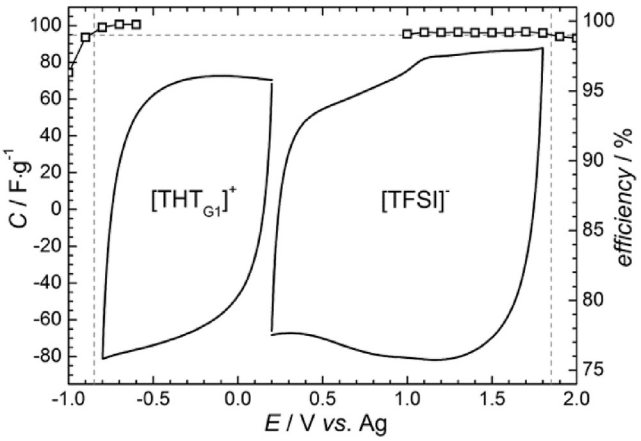

Fig. 6. Specific capacitance (line, left y-axis) and Coulombic efficiency (-□-, right y-axis) obtained by CV at 5 mV s^{-1} using an AC electrode and [THT$_{G1}$][TFSI] as electrolyte. The horizontal line dashed line represents the 99% threshold in efficiency. The vertical dashed lines mark the potential at which the efficiency falls below 99% (−0.85 V *vs*. Ag and 1.85 V *vs*. Ag for the lower and upper potentials, respectively).

electrolyte is considered stable and no significant loss of Coulombic efficiency, *via* undesirable Faradaic electron transfer decomposition reactions, is observed. As seen in Fig. 6, when used with the AC electrodes, this operative potential range is between −0.85 V *vs*. Ag and 1.85 V *vs*. Ag. The positive potential limit of 1.85 V *vs*. Ag corresponds to the anodic stability of the [TFSI]$^-$ anion and is in line with other potential limits determined for this anion [45]. The maximum potential of the [THT$_{G1}$]$^+$ cation of −0.85 V *vs*. Ag is low, particularly when compared with the apparent cathodic reduction potential of the IL (−2.15 V *vs*. Fc$^+$/Fc) as determined at a planar glassy carbon electrode. This difference in potential limits can most certainly be attributed to the differences in electrochemical setups. The electrochemical stability window is derived using inert, planar and nonporous electrodes, which feature high electrical conductivity and very low specific surface areas (like the used glassy carbon and Pt-wire) [70]. Conversely, EDLC electrodes are constructed using porous activated carbon with varying amounts of surface groups, which are able to interact in different ways with the electrolyte species. This variation in electrode structure ultimately effects the determination of electrolyte stability and is responsible for the difference in potential limits obtained by the different methods. This is another example of how the applied method influences the assessment of the stability of the electrolyte, which one has to keep in mind for the determination of the operative voltage for full cells [70,71]. Nevertheless, the actual maximum cathodic stability of the [THT$_{G1}$]$^+$ cation at the EDLC-type electrodes (−0.85 V *vs*. Ag) is very similar to previously reported literature values for three [TFSI]$^-$-based ILs with acyclic *S-alkyl-S,S*-diethylsulfonium cations (where the term *alkyl* refers to a methyl, ethyl and propyl group) [41].

To further evaluate the electrochemical behaviour, EDLCs with two AC-based composite electrodes were constructed. Using the potential limits determined previously, a maximum cell voltage of 2.6 V was selected for these tests. Due to the difference in voltage excursion on the positive and negative electrodes, an asymmetrical cell configuration with different electrode masses was selected based on Equation (1). Fig. 7a shows an exemplary CV for the investigated electrolyte completed at a scan rate of 20 mV s^{-1}. The typical rectangular shape for capacitive behaviour of an EDLC is observed and no additional current peaks, which would indicate unwanted Faradaic reactions, are present. Using this scan rate, a specific capacitance of 21 F g^{-1} is reached for the whole device. This value of capacitance is comparable to that observed for similar electrodes in pyrrolidinium-based and trialkylsulfonium-based IL electrolytes [41,45]. Fig. 7b shows the development of the specific capacitance with an increasing scan rate. At a scan rate of 200 mV s^{-1}, 33% of the initial capacitance at 5 mV s^{-1} is left. As discussed previously, at 298 K the [THT$_{G1}$][TFSI] IL has a conductivity of 3.01 mS cm^{-1} and a viscosity of 70.38 mPa s, which leads to high resistance and, therefore, poorer performance at higher rates.

The electrochemical performance of the IL was further investigated by galvanostatic cycling experiments using current densities ranging from 0.5 A g^{-1} to 2 A g^{-1} with a maximum applied operative voltage of 2.6 V (Fig. 8). The voltage profiles of the different current densities are presented in Fig. 8d; a comparison of the voltage profile of the investigated [THT$_{G1}$][TFSI] IL with a standard organic electrolyte (1 mol dm^{-3} Et_4NBF_4 in PC) using a current density of 1 A g^{-1} is presented in Figure S8. In the cycling experiments, the Coulombic efficiency reaches values close to 100%. Furthermore, the EDLC is very stable upon cycling at the different current densities, indicating that no electrolyte degradation is taking place. Both the *ESR* and the specific capacitance show a minor decrease in the first 1000 cycles stabilizing at values of 28.5 Ω cm^2 and 18.7 F g^{-1}, respectively. At 2 A g^{-1} the specific capacitance decreases to 14.3 F g^{-1}, while at 5 A g^{-1} the system becomes completely polarized. Again, the relatively high viscosity of the IL at room temperature limits the possible electrochemical performance of the EDLC at higher current densities. The voltage profiles show a linear increase/decrease of the voltage upon charging/discharging, thus, no contribution of faradaic processes are involved in the storage processes of the investigated combination of materials. Upon reversing the applied current, a large

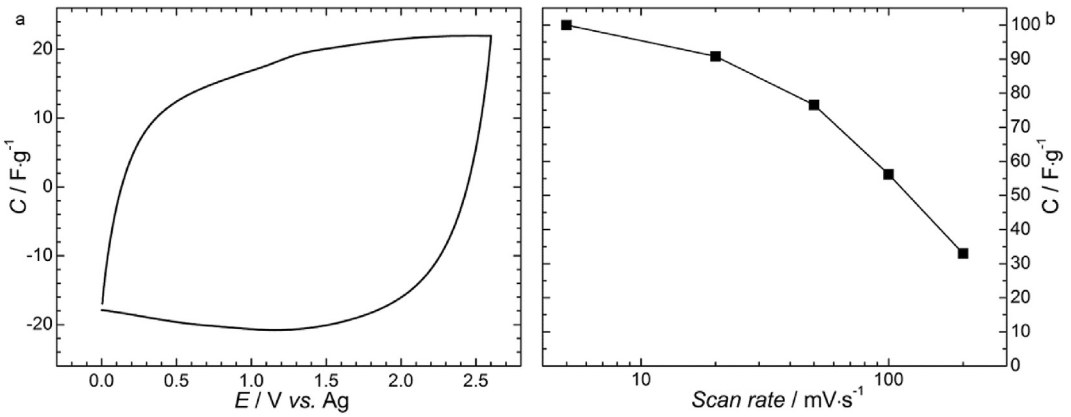

Fig. 7. (a) Cyclic voltammetry of the investigated [THT$_{G1}$][TFSI] electrolyte at a scan rate of 20 mV s^{-1}. (b) Capacitance retention for scan rates ranging from 5 to 200 mV s^{-1}.

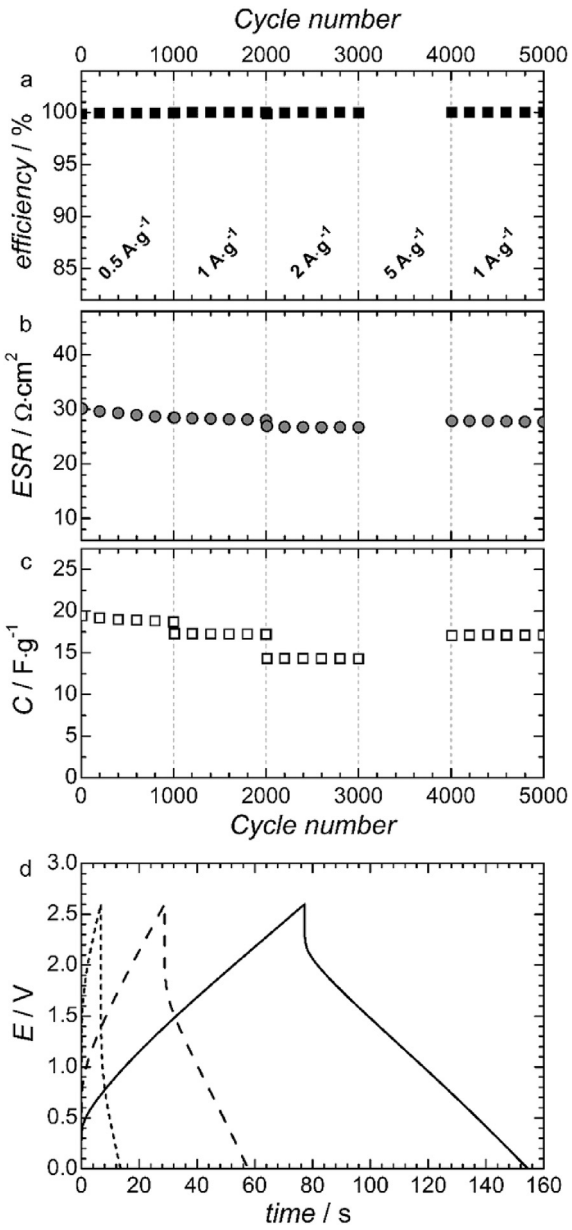

Fig. 8. Evolution of Coulombic efficiency (a, ■), *ESR* (b, ○) and specific capacitance (c, □) of EDLCs containing the investigated [THT_{G1}][TFSI] electrolyte using a maximum voltage of 2.6 V and current densities from 0.5 to 5 A g^{-1}. (d) Voltage profiles of the investigated [THT_{G1}][TFSI] electrolyte at 0.5 A g^{-1} (—), 1 A g^{-1} (– –) and 2 A g^{-1} (---).

Ohmic drop is visible attributed to the high resistance of the EDLC due to the high viscosity of the IL at room temperature. Compared to an organic electrolyte, 1 mol dm^{-3} Et_4NBF_4 in PC (Figure S8), the charge/discharge time of the investigated [THT_{G1}][TFSI] IL is about half of the value of the organic electrolyte and the Ohmic drop upon current reversal is higher for the investigated [THT_{G1}][TFSI] IL. Keeping the difference in conductivity and viscosity of the two electrolytes in mind (3.01 mS cm^{-1}/70.38 mPa s and 13 mS cm^{-1}/2.6 mPa s for [THT_{G1}][TFSI] and 1 mol dm^{-3} Et_4NBF_4 in PC, respectively), this outcome is not surprising [21].

4. Conclusions

In this work, we have reported the synthesis and chemical-physical properties of the alkyl and ether-functionalised cyclic sulfonium ILs, [THT_4][TFSI] and [THT_{G1}][TFSI], respectively. An assessment of the thermal properties revealed both ILs exhibit wide liquid range temperatures, particularly in sub-ambient temperatures. Physical characterisation of the density and transport properties, viscosity and conductivity, of the ILs showed similarities between commonly used, and similarly sized, ILs like those based on the pyrrolidinium cation with the $[TFSI]^-$ anion. Additionally, these measurements demonstrated how small structural modifications, like the introduction of an ethereal oxygen onto the cation, may be used to improve or fine-tune some desired characteristics. Specifically, the introduction of the ether-appendage was found to reduce the measured viscosity and increase the conductivity of the IL, relative to the alkyl-functionalised analogue. Moreover, this structural modification was found to have no negative implications on the thermal stability of the IL nor the electrochemical stability window of the IL, as measured by CV at a glassy carbon working electrode.

Initial EDLC testing using the novel ether-functionalised IL, [THT_{G1}][TFSI], as a solvent-free electrolyte with AC-composite electrodes was completed to inspect the potential application of this material. The electrochemical performance of these EDLCs was found to be comparable to that of other solvent-free EDLC systems, *i.e.* using an electrolyte based on the pyrrolidinium-cation. However, the operative voltage of the investigated devices appears lower than that of many other solvent-free EDLCs and power outputs are limited by sluggish transport properties at ambient temperatures. Taking these points into account, the increment of the operative voltage and improvement of transport properties appear as the main goals to achieve in order to take full advantage of the favourable properties of ILs as electrolytes. Furthermore, also the behaviour at low temperature of these innovative solvent-free EDLCs should be investigated.

Acknowledgements

The authors would like to gratefully acknowledge the funding from EPSRC (EP/L505262/1) and Innovate UK for the Practical Lithium-Air Batteries project (project number: 101577). S.M. would like to gratefully acknowledge the funding from EPSRC (project reference: S3802ASA). A.B. and C.S. would like to thank the Bundesministerium für Bildung und Forschung (BMBF) within the project IES (contract number: 03EK3010) for the financial support. We gratefully appreciated the supply of materials by Norit Activated Carbon Holding (DLC Super 30) and Imerys (Super C65).

Appendix A. Supplementary data

Supporting data are openly available on Queen's University Research Portal: http://pure.qub.ac.uk/portal/en/datasets/search.html. Supplementary data related to this article can be found at http://dx.doi.org/10.1016/j.jpowsour.2016.06.085.

References

[1] P. Simon, Y. Gogotsi, Nat. Mater. 7 (2008) 845–854.
[2] J.R. Miller, A.F. Burke, Electrochem. Soc. Interface 17 (2008) 53–57.
[3] F. Béguin, V. Presser, A. Balducci, E. Frackowiak, Adv. Mater. (Weinheim, Ger.) 26 (2014) 2219–2251.
[4] G. Wang, L. Zhang, J. Zhang, Chem. Soc. Rev. 41 (2012) 797–828.
[5] L.L. Zhang, X.S. Zhao, Chem. Soc. Rev. 38 (2009) 2520–2531.
[6] P. Sharma, T.S. Bhatti, Energy Convers. Manage. 51 (2010) 2901–2912.
[7] R. Burt, G. Birkett, X.S. Zhao, Phys. Chem. Chem. Phys. 16 (2014) 6519–6538.
[8] M. Arulepp, J. Leis, M. Lätt, F. Miller, K. Rumma, E. Lust, A.F. Burke, J. Power Sources 162 (2006) 1460–1466.
[9] Y. Korenblit, M. Rose, E. Kockrick, L. Borchardt, A. Kvit, S. Kaskel, G. Yushin, ACS Nano 4 (2010) 1337–1344.
[10] D.N. Futaba, K. Hata, T. Yamada, T. Hiraoka, Y. Hayamizu, Y. Kakudate, O. Tanaike, H. Hatori, M. Yumura, S. Iijima, Nat. Mater. 5 (2006) 987–994.

[11] B. Xu, F. Wu, R. Chen, G. Cao, S. Chen, G. Wang, Y. Yang, J. Power Sources 158 (2006) 773–778.
[12] Y. Tao, X. Xie, W. Lv, D.-M. Tang, D. Kong, Z. Huang, H. Nishihara, T. Ishii, B. Li, D. Golberg, F. Kang, T. Kyotani, Q.-H. Yang, Sci. Rep. 3 (2013) 2975.
[13] H. Wei, C. He, J. Liu, H. Gu, Y. Wang, X. Yan, J. Guo, D. Ding, N.Z. Shen, X. Wang, S. Wei, Z. Guo, Polymer 67 (2015) 192–199.
[14] Y. Wang, H. Wei, J. Wang, J. Liu, J. Guo, X. Zhang, B.L. Weeks, T.D. Shen, S. Wei, Z. Guo, J. Mater. Chem. A 3 (2015) 20778–20790.
[15] A. Burke, M. Miller, J. Power Sources 196 (2011) 514–522.
[16] T. Abdallah, D. Lemordant, B. Claude-Montigny, J. Power Sources 201 (2012) 353–359.
[17] A. Balducci, R. Dugas, P.L. Taberna, P. Simon, D. Plée, M. Mastragostino, S. Passerini, J. Power Sources 165 (2007) 922–927.
[18] C. Arbizzani, M. Biso, D. Cericola, M. Lazzari, F. Soavi, M. Mastragostino, J. Power Sources 185 (2008) 1575–1579.
[19] A. Lewandowski, A. Olejniczak, M. Galinski, I. Stepniak, J. Power Sources 195 (2010) 5814–5819.
[20] A. Brandt, S. Pohlmann, A. Varzi, A. Balducci, S. Passerini, MRS Bull. 38 (2013) 554–559.
[21] A. Krause, A. Balducci, Electrochem. Commun. 13 (2011) 814–817.
[22] A. Brandt, A. Balducci, J. Power Sources 250 (2014) 343–351.
[23] S. Pohlmann, T. Olyschläger, P. Goodrich, J.A. Vicente, J. Jacquemin, A. Balducci, Electrochim. Acta 153 (2015) 426–432.
[24] V. Ruiz, T. Huynh, S.R. Sivakkumar, A.G. Pandolfo, RSC Adv. 2 (2012) 5591–5598.
[25] A. Brandt, P. Isken, A. Lex-Balducci, A. Balducci, J. Power Sources 204 (2012) 213–219.
[26] F. Ghamouss, A. Brugère, J. Jacquemin, J. Phys. Chem. C 118 (2014) 14107–14123.
[27] E. Coadou, L. Timperman, J. Jacquemin, H. Galiano, C. Hardacre, M. Anouti, J. Phys. Chem. C 117 (2013) 10315–10325.
[28] X. Baokou, M. Anouti, J. Phys. Chem. C 119 (2015) 970–979.
[29] Z.-B. Zhou, H. Matsumoto, K. Tatsumi, Chem. Eur. J. 12 (2006) 2196–2212.
[30] K. Tsunashima, S. Kodama, M. Sugiya, Y. Kunugi, Electrochim. Acta 56 (2010) 762–766.
[31] Z.-B. Zhou, H. Matsumoto, K. Tatsumi, Chem. Eur. J. 11 (2005) 752–766.
[32] C. Wolff, S. Jeong, E. Paillard, A. Balducci, S. Passerini, J. Power Sources 293 (2015) 65–70.
[33] H. Matsumoto, H. Sakaebe, K. Tatsumi, J. Power Sources 146 (2005) 45–50.
[34] C.-P. Lee, J.-D. Peng, D. Velayutham, J. Chang, P.-W. Chen, V. Suryanarayanan, K.-C. Ho, Electrochim. Acta 114 (2013) 303–308.
[35] C. Xi, Y. Cao, Y. Cheng, M. Wang, X. Jing, S.M. Zakeeruddin, M. Grätzel, P. Wang, J. Phys. Chem. C 112 (2008) 11063–11067.
[36] Q. Zhang, S. Liu, Z. Li, J. Li, Z. Chen, R. Wang, L. Lu, Y. Deng, Chem. Eur. J. 15 (2009) 765–778.
[37] L. Guo, X. Pan, C. Zhang, M. Wang, M. Cai, X. Fang, S. Dai, J. Mol. Liq. 158 (2011) 75–79.
[38] L. Guo, X. Pan, C. Zhang, W. Liu, M. Wang, X. Fang, S. Dai, Sol. Energy 84 (2010) 373–378.
[39] S. Luo, Z. Zhang, L. Yang, Chin. Sci. Bull. 53 (2008) 1337–1342.
[40] A. Bhattacharjee, A. Luís, J.H. Santos, J.A. Lopes-da-Silva, M.G. Freire, P.J. Carvalho, J.A.P. Coutinho, Fluid Phase Equilib. 381 (2014) 36–45.
[41] A.J.R. Rennie, V.L. Martins, R.M. Torresi, P.J. Hall, J. Phys. Chem. C 119 (2015) 23865–23874.
[42] H.-B. Han, J. Nie, K. Liu, W.-K. Li, W.-F. Feng, M. Armand, H. Matsumoto, Z.-B. Zhou, Electrochim. Acta 55 (2010) 1221–1226.
[43] A. Krause, P. Kossyrev, M. Oljaca, S. Passerini, M. Winter, A. Balducci, J. Power Sources 196 (2011) 8836–8842.
[44] M. Lazzari, F. Soavi, M. Mastragostino, J. Power Sources 178 (2008) 490–496.
[45] S. Pohlmann, C. Ramirez-Castro, A. Balducci, J. Electrochem. Soc. 162 (2015) A5020–A5030.
[46] P. Kurzweil, M. Chwistek, J. Power Sources 176 (2008) 555–567.
[47] R.S. Kühnel, N. Böckenfeld, S. Passerini, M. Winter, A. Balducci, Electrochim. Acta 56 (2011) 4092–4099.
[48] L. Chancelier, A.O. Diallo, C.C. Santini, G. Marlair, T. Gutel, S. Mailley, C. Len, Phys. Chem. Chem. Phys. 16 (2014) 1967–1976.
[49] P. Bonhôte, A.P. Dias, N. Papageorgiou, K. Kalyanasundaram, M. Grätzel, Inorg. Chem. 35 (1996) 1168–1178.
[50] A. Martinelli, A. Matic, P. Jacobsson, L. Börjesson, A. Fernicola, B. Scrosati, J. Phys. Chem. B 113 (2009) 11247–11251.
[51] Z.-B. Zhou, H. Matsumoto, K. Tatsumi, Chem. Eur. J. 10 (2004) 6581–6591.
[52] T. Belhocine, S.A. Forsyth, H.Q.N. Gunaratne, M. Nieuwenhuyzen, P. Nockemann, A.V. Puga, K.R. Seddon, G. Srinivasan, K. Whiston, Green Chem. 13 (2011) 3137.
[53] J. Jacquemin, P. Husson, A.A.H. Padua, V. Majer, Green Chem. 8 (2006) 172–180.
[54] C.A. Angell, Ionic liquids in the temperature range 150-1500 K: patterns and problems, in: Molten Salts and Ionic Liquids, John Wiley & Sons, Inc., 2010, pp. 1–24.
[55] Z.J. Chen, T. Xue, J.-M. Lee, RSC Adv. 2 (2012) 10564–10574.
[56] A. Orita, K. Kamijima, M. Yoshida, L. Yang, J. Power Sources 195 (2010) 6970–6976.
[57] D.R. MacFarlane, M. Forsyth, E.I. Izgorodina, A.P. Abbott, G. Annat, K. Fraser, Phys. Chem. Chem. Phys. 11 (2009) 4962–4967.
[58] K. Ueno, H. Tokuda, M. Watanabe, Phys. Chem. Chem. Phys. 12 (2010) 1649–1658.
[59] W. Xu, E.I. Cooper, C.A. Angell, J. Phys. Chem. B 107 (2003) 6170–6178.
[60] K.J. Fraser, E.I. Izgorodina, M. Forsyth, J.L. Scott, D.R. MacFarlane, Chem. Commun. (2007) 3817–3819.
[61] M. Galiński, A. Lewandowski, I. Stępniak, Electrochim. Acta 51 (2006) 5567–5580.
[62] S. Fang, L. Yang, C. Wei, C. Peng, K. Tachibana, K. Kamijima, Electrochem. Commun. 9 (2007) 2696–2702.
[63] T. Yim, H.Y. Lee, H. Kim, J. Mun, S. Kim, S.M. Oh, Y.G. Kim, Bull. Korean Chem. Soc. 28 (2007) 1567–1572.
[64] M. Montanino, F. Alessandrini, S. Passerini, G.B. Appetecchi, Electrochim. Acta 96 (2013) 124–133.
[65] A.M. O'Mahony, D.S. Silvester, L. Aldous, C. Hardacre, R.G. Compton, J. Chem. Eng. Data 53 (2008) 2884–2891.
[66] K. Tsunashima, Y. Sakai, M. Matsumiya, Electrochem. Commun. 39 (2014) 30–33.
[67] K. Tsunashima, Y. Ono, M. Sugiya, Electrochim. Acta 56 (2011) 4351–4355.
[68] K. Tsunashima, M. Sugiya, Electrochem. Commun. 9 (2007) 2353–2358.
[69] P. Bonhôte, A.-P. Dias, N. Papageorgiou, K. Kalyanasundaram, M. Grätzel, Inorg. Chem. 35 (1996) 1168–1178.
[70] K. Xu, S.P. Ding, T.R. Jow, J. Electrochem. Soc. 146 (1999) 4172–4178.
[71] D. Weingarth, H. Noh, A. Foelske-Schmitz, A. Wokaun, R. Kötz, Electrochim. Acta 103 (2013) 119–124.

Please cite this article in press as: A.R. Neale, et al., Journal of Power Sources (2016), http://dx.doi.org/10.1016/j.jpowsour.2016.06.085